Journal of The Electrochemical Society, **162** (1) F92-F97 (2015)
0013-4651/2015/162(1)/F92/6/$31.00 © The Electrochemical Society

Construction of 3D Pt Catalysts Supported on Co-Doped SnO_2 Nanourchins for Methanol and Ethanol Electrooxidation

Hulin Zhang,[a,z] Chenguo Hu,[b] Cuiling Zhang,[b] Kaiyou Zhang,[b] Mingjun Wang,[b] Yong Ding,[c] and Yuan Lin[a,d,z]

[a]*State Key Laboratory of Electronic Thin Film and Integrated Devices, University of Electronic Science and Technology of China, Chengdu, Sichuan 610054, People's Republic of China*
[b]*Department of Applied Physics, Chongqing University, Chongqing 400044, People's Republic of China*
[c]*School of Materials Science and Engineering, Georgia Institute of Technology, Atlanta, Georgia 30332-0245, USA*
[d]*Institute of Electronic and Information Engineering in Dongguan, University of Electronic Science and Technology of China, Dongguan, 523808 Guangdong, People's Republic of China*

Pt nanoparticles on Co-doped SnO_2 nanostructures have been synthesized and used for methanol and ethanol electrooxidation. The hierarchical Co-SnO_2 nanostructure with urchin-like morphology, self-assembled from numerous thin nanoneedles, provides a three-demensional (3D) frame for supporting Pt nanoparticles. The as-prepared Pt/Co-SnO_2(urchin) nanocatalyst was characterized by X-ray diffraction (XRD), energy dispersive X-ray spectroscopy (EDS), X-ray photoelectron spectroscopy (XPS), field effect scanning electron microscopy (FESEM) and transmission electron microscopy (TEM). Cyclic voltammetry (CV), linear sweep voltammetry (LSV) and chronoamperometry were carried out to comparatively investigate electrochemical properties of Pt/Co-SnO_2(urchin), Pt/Co-SnO_2(flower), Pt/SnO_2 and Pt/C electrocatalysts. The urchin-shaped Pt/Co-SnO_2 electrocatalyst shows better catalytic activity and higher catalytic stability compared with the other electrocatalysts.
 [DOI: 10.1149/2.0771501jes]

Manuscript submitted September 9, 2014; revised manuscript received November 11, 2014. Published November 19, 2014.

Owing to the high energy conversion efficiency, low operating temperature, and simplicity of handing and processing of liquid fuel, the direct alcohol fuel cells (DAFCs) have been paid much attention to as green power sources especially for mobile power supply systems among the various types of fuel cell in recent decades. Methanol is usually utilized as fuel because it can be more efficiently oxidized than other small organic molecules, and ethanol is one of the most promising fuels with its low toxicity, abundance, low permeability across proton exchange membrane and high energy density.[1–3] Until now, though it has been found that a few metallic oxides have catalytic activity for alcohol electrooxidation, Pt-based electrocatalysts have been considered the most promising electrode materials for electrooxidation of methanol or ethanol due to the good electrochemical stability and favorable electrocatalytic activity.[4–6] The electrocatalysts are mainly consisted of Pt nanoparticles and a certain support material. Electrocatalyst particles are distributed on the suitable support material, which can greatly enhance the surface area and lower sintering effects, resulting in higher electrocatalytic activity for alcohol oxidation.[7]

In the most recent period, various nanostructured materials have been investigated actively as Pt electrocatalyst support because of the urgency of DAFCs' development. Carbon nanostructures are usually chosen for supporting nanoscale electrocatalyst particles in DAFCs on account of its large surface area, high electrical conductivity, and porous morphology.[4,8,9] However, this inert material (carbon) serves only as a mechanical support without any help to catalytic activity. But lately, some studies have demonstrated that the support materials may also enhance the catalytic activity, mostly using metallic oxide materials, which were named as active or promoting support.[10–13] SnO_2 has been considered as an excellent candidate for the support material because of its chemical properties. It not only can adsorb OH species at lower potential, but also can produce the electronic effect with Pt catalysts, which can facilitate the electrooxidation of alcohols with low molecular weight alcohol, such as methanol and ethanol.[14,15] In addition to its electrochemical activity, the stability of the SnO_2-based support material in electrochemical reactions is also desirable, which has been proved by Chhina's group through investigation of the oxidation resistance of supports.[16]

Although there have been some reports on Pt catalyst supported on SnO_2, it is necessary to synthesize SnO_2 nanomaterials with hierarchical structure, which can greatly improve the activities for alcohol oxidation by increasing the specific surface area and providing numerous micropores and microchannels to promote diffusion of the reactants and shorten the electronic diffusion length.[17,18] On the other hand, it is known that doping, which not only can tune the spatial structures of nanomaterials by tailoring their size, shape, and morphology, but also can adjust the surface adsorption to enhance catalytic activity.[19,20] However, there are few reports about the transition metal doping SnO_2 nanostructures with hierarchical structure used to support Pt catalyst for alcohol electrooxidation. Accordingly, it is expected that doped hierarchical tin oxide nanostructures with porous structures and larger specific surface area can be applied in DAFCs.

In the present work, the prepared Co-doped SnO_2 nanostructures were employed as three-dimensional supports for loading Pt nanoparticles to assist the oxidation of methanol/ethanol. The Pt supported on Co-doped SnO_2 (Pt/Co-SnO_2) catalysts were characterized by XRD, FESEM, EDS, XPS and TEM. In addition, the performances of the electrocatalysts for methanol and ethanol electrooxidation were studied via CV, LSV, and chronoamperometry in acidic medium. The Pt/Co-SnO_2(urchin) electrocatalyst shows a higher electrochemically active surface area from the three-dimensional hierarchical structure and better performance for methanol and ethanol oxidation reaction compared with the other catalysts.

Experimental

$Na_2SnO_3 \cdot 3H_2O$, NaOH, $Co(NO_3)_2 \cdot 6H_2O$, H_2PtCl_6, $NaBH_4$, methanol and ethanol were purchased from Chongqing Chemical Reagent Company. Carbon black (Vulcan XC72R) was from CABOT Corp. Nafion and silver paste were purchased from Sigma-Aldrich and SPI Supplies. All chemicals were of analytical grade and used as received. Deionized water was used throughout.

The Co-SnO_2 nanostructures were prepared by a hydrothermal method.[21] In a typical synthesis, 0.4 g of $Na_2SnO_3 \cdot 3H_2O$, 0.4 g of NaOH and a certain weight of $Co(NO_3)_2 \cdot 6H_2O$ (the Co molar content in samples was 0, 1 and 3 mol%) were mixed with 10 mL deionized water and 10 mL absolute ethanol in a beaker, followed by hydrothermal treatment at 200°C for 24 h in a Teflon-lined autoclave after magnetic stirring for 5 min. Then the autoclave was allowed to cool down naturally. Subsequently, the precipitate was obtained by centrifugation and washed with deionized water and ethanol several times. After that, the hydrothermal product was dried in air.

Pt nanoparticles supported on Co-SnO_2 nanostructures were synthesized at room temperature by chemical reduction of $H_2PtCl_6.6H_2O$ using $NaBH_4$. Briefly, a mixture of 0.03 g Co-SnO_2 nanocrystals and 0.009 g $H_2PtCl_6.6H_2O$ and 10 mL deionized water was added into a

[z]E-mail: zhangd198710@gmail.com; linyuan@uestc.edu.cn

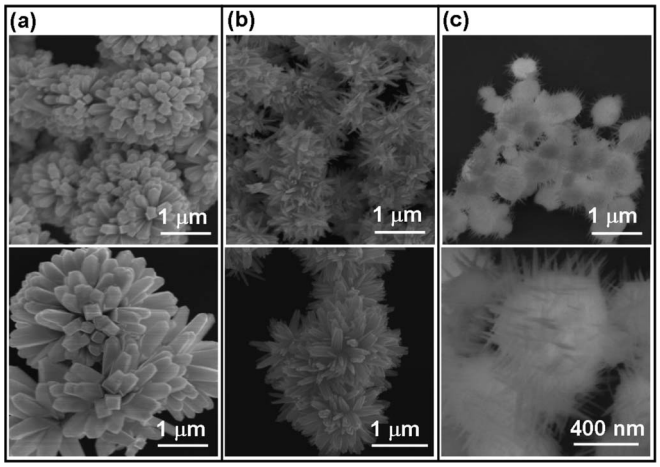

Figure 1. FESEM images of the synthesized SnO_2 nanostructures with different content of doping Co. (a) Flower-like SnO_2 without doping Co. (b) Flower-like Co-SnO_2 with 1% doping Co. (c) Urchin-like Co-SnO_2 with 3% doping Co.

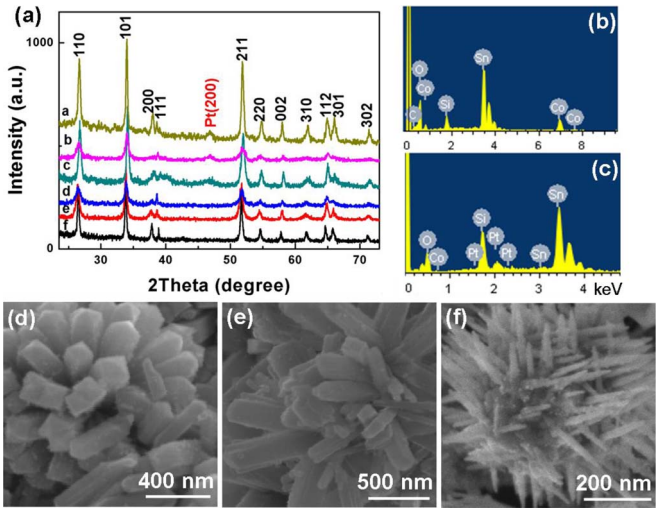

Figure 2. Phase and morphology characterizations of Pt/Co-SnO_2 catalysts. (a) XRD patterns of Co-SnO_2 nanomaterials and Pt/Co-SnO_2 catalysts. (b-c) EDS spectra of Co-SnO_2 after and before being deposited by Pt. (d-f) FESEM images of Pt/SnO_2 (d), Pt/Co-SnO_2(flower) (e) and Pt/Co-SnO_2(urchin) (f).

beaker. Then 0.01 M $NaBH_4$ solution was instilled under continuous magnetic stirring until the color of the solution remained unchanged. Finally, the black Pt/Co-SnO_2 nanostructures were washed with deionized water and ethanol.

The dispersed Pt/Co-SnO_2 ethanol solution with volume of 10 μL was employed to coat the graphite electrode which had been polished and cleaned. After dried, 5 μL of 0.5 wt% Nafion was dropped on the surface of electrode so as to immobilize the Pt/Co-SnO_2 nanostructures on the electrode and to enhance the anti-interference ability. In the end, the electrodes were covered by epoxy resin leaving an open area of 4 mm × 5 mm. The Pt loading on each electrode was 0.1 mg cm^{-2}. To compare catalysis of the Pt/Co-SnO_2 electrocatalysts with other common Pt-based catalyst, Pt supported on carbon black (Pt/C) was prepared [24] as the reported with the same Pt loading.

For all samples, phase analysis and chemical composition was structurally characterized by XRD (BDX3200), EDS (Oxford) and XPS (ESCALAB MKII using Mg Ka as the exciting source) at room temperature. The morphologies were observed by FESEM (FEI Nova 400) and TEM (TF30). CHI660D electrochemical analyzer was employed for electrochemical measurements, which was performed in a conventional three-electrode electrochemical cell. Pt foil and Ag/AgCl (saturated KCl) were used as the counter and reference electrodes, respectively. The current density presented in this paper has been normalized with real surface area. All the experiments were carried out at room temperature (20°C).

Results and Discussion

The typical FESEM images of the synthesized SnO_2 nanostructures with different content of doping Co are presented in Fig. 1, with the corresponding high resolution FESEM images of the Co-SnO_2 revealed in the bottom of Fig. 1. The pure SnO_2 nanocrystal and the SnO_2 nanostructure prepared with 1% Co present flower-shaped morphology in Fig. 1a and 1b, respectively. Although the flower-like structures of the pure SnO_2 and the SnO_2 doped with 1% Co are consisted of nanorods, the diameter of the nanorods for SnO_2 doped with 1% Co is smaller. Figure 1c displays the urchin-like structure of SnO_2 doped with 3% Co. The nanourchins are formed by extremely thin nanoneedles, which gathered together, rooted in one center and self-assembled into the beautiful urchin-shaped 3D hierarchical nanostructure.

XRD patterns of the prepared Co-SnO_2 nanocrystals and Pt/Co-SnO_2 electrocatalysts are comparatively shown in Fig. 2a. Crystalline features are evident in all XRD profiles. Clearly, curve a, b and c originated from the Pt/Co-SnO_2 nanocrystals have an additional peak at the 2θ of 46.3°, compared with that of the Co-SnO_2 nanostructures (curve d, e and f). Through verification, nearly all the peaks can be well indexed to tetragonal SnO_2 (JCPDS 41-1445). Exceptionally, the peak at the 2θ of 46.3° corresponds to the (200) of the face-centered cubic Pt, suggesting that platinum was successfully deposited on the Co-SnO_2 nanomaterials. Fig. 2b and 2c, respectively, illustrate typical EDS spectra of the Co-SnO_2 after and before being deposited by Pt, revealing that the samples contain Pt in addition to tin, oxygen and cobalt after being deposited. The FESEM images of the Pt/Co-SnO_2 catalyst are shown in Fig. 2d, 2e and 2f, evidently indicating Pt nanoparticles were uniformly covered on Co-SnO_2 nanostructures. Especially, Co-SnO_2 nanourchins with 3% doping Co have a delicate 3D spatial structure, resulting in Pt nanoparticles uniformly growing on the surface of thin nanoneedles. Hence, it is likely that Pt/Co-SnO_2 nanourchins have an excellent catalytic ability.

The purity and composition of the Pt/Co-SnO_2 nanourchins are studied by XPS analysis. The XPS spectra of the sample are plotted in Fig. 3. The signal of Pt is detected in the XPS survey spectrum (Fig. 3a). Fig. 3b–3e shows the detailed high-resolution spectra of the product. Especially, the two peaks at 70.9 eV and 74.3 eV correspond to the Pt $4f_{7/2}$ and $4f_{5/2}$, respectively. The XPS analysis further confirmed that Pt was successfully deposited on the Co-SnO_2 nanourchins.

To obtain more details of the Pt/Co-SnO_2 nanourchins, TEM images in Fig. 4a and 4b illuminate numerous Pt particles grown on nanoneedles uniformly, in good agreement with the FESEM results. For the further observation of the details of Pt/Co-SnO_2 nanourchins, a HRTEM image and a STEM image are exhibited in Fig. 4c and 4d, respectively. It can be seen that Pt particles of about 5 to 8 nm located on nanoneedles. Energy-dispersive X-ray spectrometry (EDS) mapping analysis of elements Pt, Co, Sn and O (shown in Fig. 4f–4i, respectively) from a select area displayed in Fig. 4e confirmed that Pt dispersed on Co-SnO_2 nanourchins.

Fig. 5a presents the CV curves of the Pt/Co-SnO_2(urchin)/G, Pt/Co-SnO_2(flower)/G, Pt/SnO_2/G and Pt/C electrodes (with the same geometric area) recorded in 0.5 M H_2SO_4 solution. In the acid medium, there are two peaks at −0.09 and 0.04 V for the four electrodes, which are associated with hydrogen adsorption/desorption process in the anodic scan. However, it is noteworthy that all the peaks of Pt/Co-SnO_2(urchin)/G electrode are stronger than that of Pt/Co-SnO_2(flower)/G, Pt/SnO_2/G and Pt/C electrodes, suggesting the Pt/Co-SnO_2(urchin) electrocatalyst has higher catalytic activity. Furthermore, according to the area of hydrogen adsorption/desorption peaks, the electrochemical active surface (EAS) was calculated.[22,23]

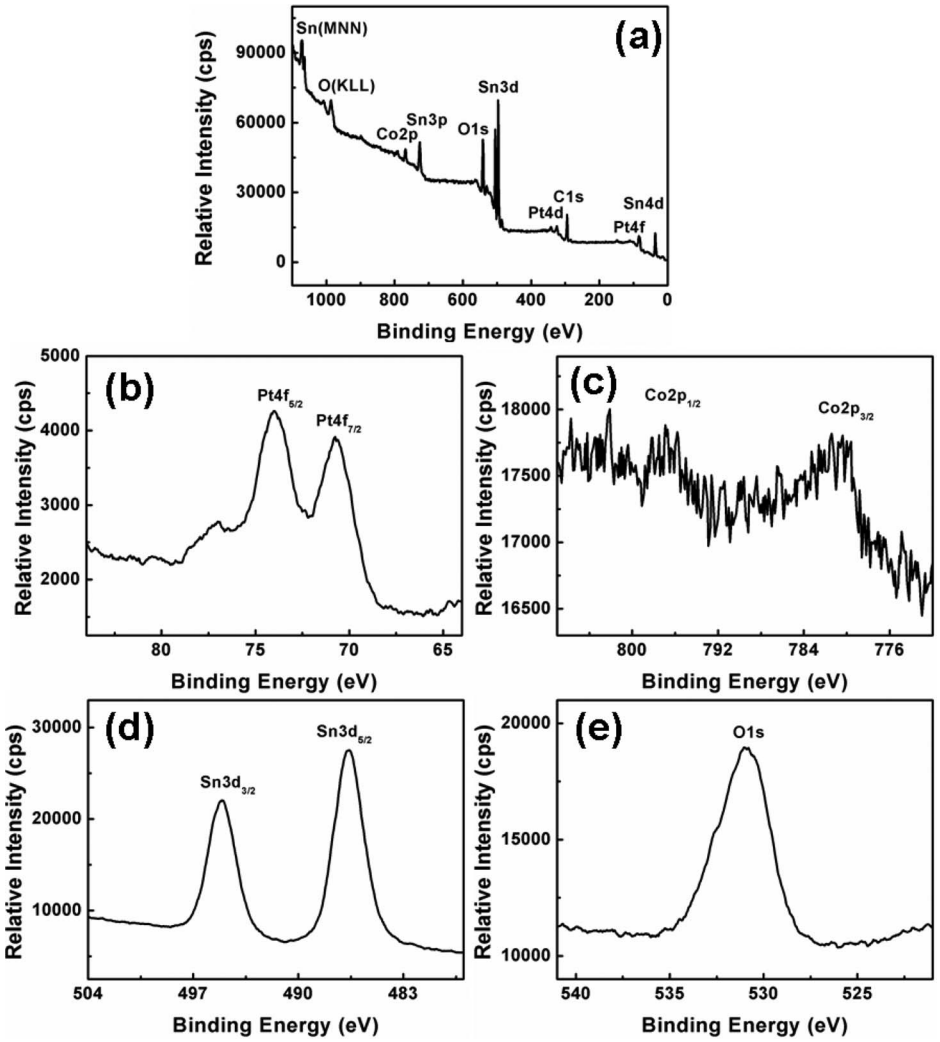

Figure 3. XPS spectra of the urchin-shaped Pt/Co-SnO2 nanostructure. (a) a typical survey spectrum. (b) Pt 4f core level. (c) Co 2p core level. (d) Sn 3d core level. (e) O 1s core level.

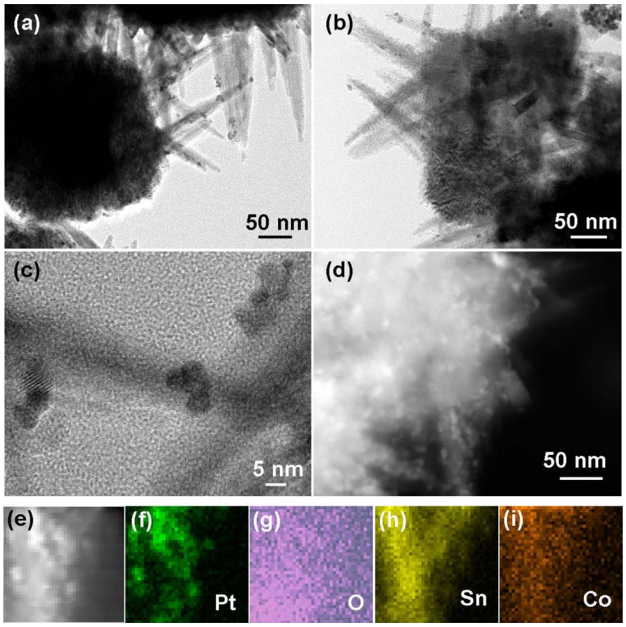

Figure 4. TEM characterization of Pt/Co-SnO_2(urchin). (a-b) TEM images of Pt/Co-SnO_2(urchin). (c) HRTEM image of Pt/Co-SnO_2(urchin). (d) STEM image of Pt/Co-SnO_2(urchin). (e-i) EDS mapping images of Pt/Co-SnO_2(urchin).

The EAS is 89.7 $m^2\ g^{-1}$ for Pt/Co-SnO_2(urchin), 77.3 $m^2\ g^{-1}$ for Pt/Co-SnO_2(flower), 45.4 $m^2\ g^{-1}$ Pt/SnO_2 and 38.5 $m^2\ g^{-1}$ for Pt/C in acid media, implying the delicate 3D hierarchical structure of Pt/Co-SnO_2(urchin) catalyst provides more active sites for Pt deposition. The result is in accord with the aforementioned FESEM and TEM characterizations, loading to an effective electrocatalysis due to the multi-dimensional structure of the Pt/Co-SnO_2(urchin) catalyst.

The performances of the Pt/Co-SnO_2(urchin), Pt/Co-SnO_2 (flower), Pt/SnO_2 and Pt/C electrocatalysts for methanol and ethanol electrooxidation in acid media are comparatively depicted in Fig. 5b and 5c, respectively, indicating that these electrocatalysts are active for methanol and ethanol oxidation. The concise comparisons of the electrochemical performances of electrocatalysts for alcohol electrooxidation are illustrated in Table I. Not surprisingly, the Pt/Co-SnO_2(urchin) electrocatalyst with 3D hierarchical structure self-assembled from numerous thin nanoneedles has a higher current density and a larger reaction surface than other catalysts though all the electrodes have reached the same apparent geometric area, which is consistent with the comparison of EAS. Compared with other electrocatalysts for methanol and ethanol electrooxidation, it is found that the Pt/Co-SnO_2(urchin) nanocatalyst exhibits not only higher current densities, but also lower onset potentials. In addition, the ratio of the forward scan peak current density (I_f) to the backward scan peak current density (I_b), i.e., I_f/I_b, can be used to describe the catalyst tolerance to carbonaceous species accumulation.[24] A higher ratio indicates preferable oxidation of alcohol to CO_2

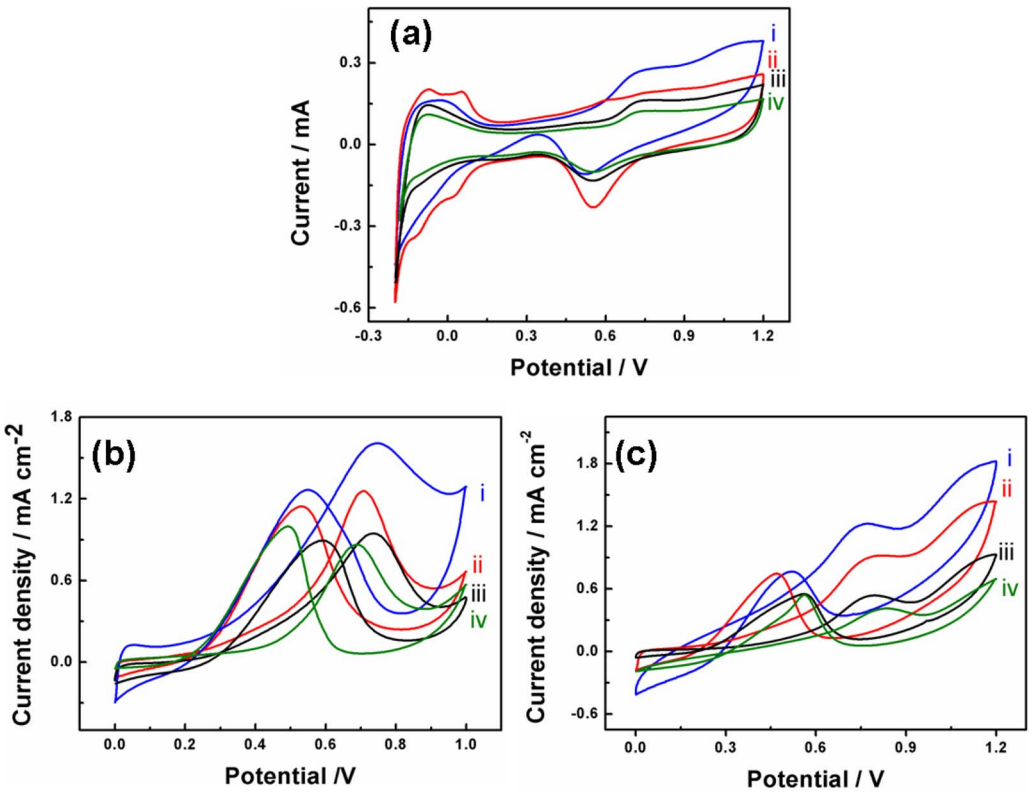

Figure 5. CV characterization of Pt/Co-SnO_2 catalysts. CVs of the Pt/Co-SnO_2(urchin)/G (i), Pt/Co-SnO_2(flower)/G (ii), Pt/SnO_2/G (iii) and Pt/C/G (iv) in 0.5 M H_2SO_4 (a), 0.5 M H_2SO_4 containing 1.0 M CH_3OH (b), or 1.0 M C_2H_5OH (c) with a sweep rate of 50 mVs^{-1}.

during the forward scan and relatively less carbonaceous residues on the surface of the catalyst. In our electrochemical characterizations, the ratio was 1.26, 1.1, 1.05 and 0.87 for the Pt/Co-SnO_2(urchin), Pt/Co-SnO_2(flower), Pt/SnO_2 and Pt/C catalyst in the methanol solution, respectively. While, the ratio was 1.5, 1.24, 0.98 and 0.79 for the Pt/Co-SnO_2(urchin), Pt/Co-SnO_2(flower), Pt/SnO_2 and Pt/C catalyst in the ethanol solution, respectively, as is shown in Table I. This indicates the multi-dimensional structure of Pt/Co-SnO_2 (urchin) catalyst presents a better catalysis to electrooxidation for methanol and ethanol. The results suggest that the spatial structure of Pt/Co-SnO_2(urchin) catalyst presents a favorable electrocatalysis for methanol and ethanol oxidation.

To further study the electrocatalysis, LSVs at very slow potential scan rate of 5 mVs-1 were carried out, as plotted in Fig. 6. It is observed that the peak current densities on the three electrodes for methanol and ethanol electrooxidation are in the order of Pt/Co-SnO_2(urchin)/G > Pt/Co-SnO_2(flower)/G > Pt/SnO_2/G > Pt/C/G. Clearly, the Pt/Co-SnO_2(urchin)/G electrode reveals a much higher oxidation current density than other electrodes from the quasi-steady-state polarization curves in acid media. The results observed here imply that the uniform distribution of Pt nanoparticles growing on the hierarchical Co-SnO_2 nanourchins can improve greatly catalytic activity toward alcohol electrooxidation, which is in accordance with the CV studies above.

The superior catalysis for methanol and ethanol electrooxidation has been achieved on the Pt/Co-SnO_2(urchin)/G electrode, which can be owning to the fact that Pt particles uniformly cover on the specific nanourchins and consequently form into a 3D hierarchical catalyst with a larger electrochemical active surface. Moreover, the extremely thin nanoneedles on Pt/Co-SnO_2(urchin) serve as radial channels and provide tremendous amount of pores, which can greatly facilitate the diffusion of the liquid/gaseous reactants between catalyst layers, leading to reduction of liquid sealing effect distinctly. Actually, the reduction of liquid sealing effect in turn enlarges the active surface area for electrochemical reactions.[25] On the other hand, the poisoning of Pt effectively decreases due to that Co-SnO_2 is proposed to improve the relaxation of CO adsorption on Pt active sites, which stems from the modification of electronic band structure of Pt and the interaction between Pt and Co-SnO_2.[26]

It is known that the electrocatalytic stability is important for alcohol oxidation in DAFCs. To give an obvious comparison of catalytic stability, Fig. 7 shows chronoamperometric curves of the four electrodes for methanol and ethanol electrooxidation. A current density decay is observed on all the electrodes in both methanol and ethanol

Table I. Comparison of the performances of the Pt/Co-SnO_2 electrodes (Co content: 0, 1 and 3 mol%) and Pt/C electrode.

	Onset Potential (V)		Peak current density ($mA\ cm^{-2}$)		I_f/I_b ratio	
Electrodes	methanol	ethanol	methanol	ethanol	methanol	ethanol
Pt/Co-SnO_2(urchin)	0.30	0.31	1.61	1.22	1.26	1.5
Pt/Co-SnO_2(flower)	0.31	0.33	1.26	0.94	1.1	1.24
Pt/SnO_2	0.37	0.35	0.94	0.54	1.05	0.98
Pt/C	0.32	0.34	0.85	0.44	0.87	0.79

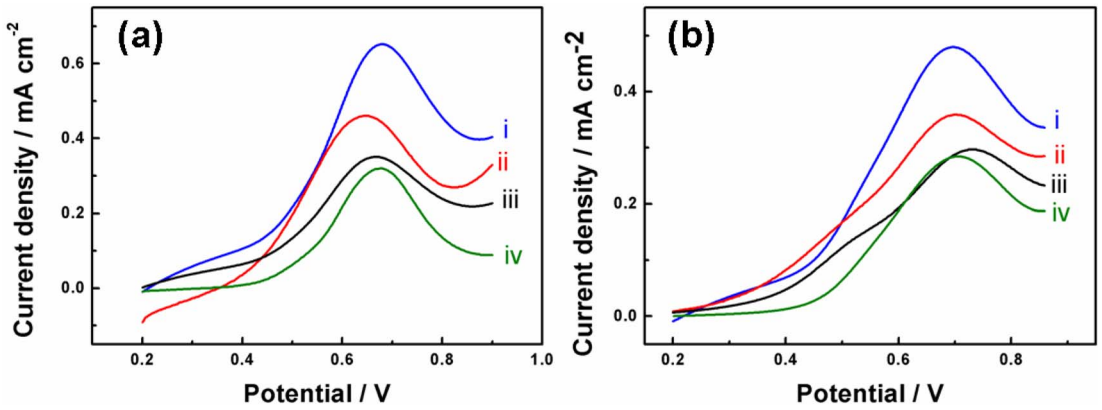

Figure 6. LSVs of the Pt/Co-SnO_2(urchin)/G (i), Pt/Co-SnO_2(flower)/G (ii), Pt/SnO_2/G (iii) and Pt/C/G (iv) in 0.5 M H_2SO_4 containing 1.0 M CH_3OH (a) or 1.0 M C_2H_5OH (b) with a sweep rate of 5 mVs^{-1}.

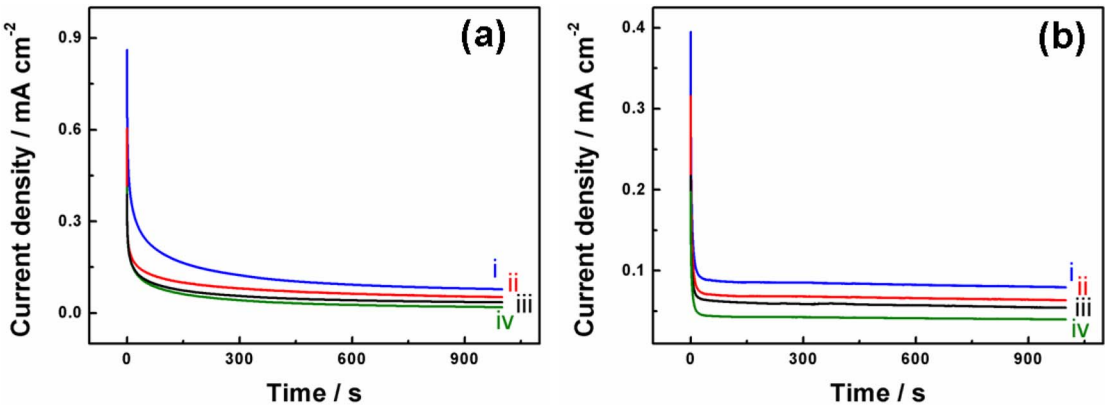

Figure 7. Chronoamperometry diagrams of the Pt/Co-SnO_2(urchin)/G (i), Pt/Co-SnO_2(flower)/G (ii), Pt/SnO_2/G (iii) and Pt/C/G (iv) in 0.5 M H_2SO_4 containing 1.0 M CH_3OH (a) or 1.0 M C_2H_5OH (b) measured at 0.7 V for 1000 seconds.

electrooxidation reaction with experimental time prolonging. However, the Pt/Co-SnO_2(urchin)/G shows a moderate decrease of current density. The current densities drop first and then reach a nearly constant over the experimental period. The ultimate steady current density on the Pt/Co-SnO_2(urchin)/G is much higher than that on the Pt/Co-SnO_2(flower)/G, on the Pt/SnO_2/G and on the Pt/C/G, as shown in Fig. 7a and 7b. Besides, the higher initial current density is achieved on the Pt/Co-SnO_2(urchin)/G electrode, which means a greater number of active sites available for oxidation. These results suggest the Pt/Co-SnO_2(urchin) catalyst has better catalytic stability and higher activity for methanol and ethanol electrooxidation than others.

Conclusions

The Co doped SnO_2 nanourchins prepared via a facile hydrothermal method were employed as supports for Pt nanoparticles to build a 3D hierarchical nanocatalyst. FESEM and TEM characterizations indicated that Pt nanoparticles with the diameter of about 5 to 8 nm are uniformly covered on the Co-SnO_2 nanostructures. Due to the perfect spatial structure of the Co-SnO_2 nanourchin support for well-distributed Pt particles, the Pt/Co-SnO_2(urchin) catalyst achieves a larger active surface area than the Pt/Co-SnO_2(flower), Pt/SnO_2 and Pt/C catalysts. Through a succession of electrochemical measurements, it is demonstrated that the Pt/Co-SnO_2(urchin) catalyst shows higher electrocatalytic activity and better stability for methanol and ethanol electrooxidation in acid media as a result of the delicate 3D structure for a better diffusion of liquid reactants. Based on our findings, Co doped SnO_2 nanourchins appear to be a promising material as a favorable support for Pt loading in DAFCs.

Acknowledgments

This work was supported by the National Basic Research Program of China (973 Program) under Grant No. 2015CB351905, National Natural Science Foundation of China (No. 51172036), and the Guangdong Innovative Research Team Program (No. 201001D0104713329).

References

1. S. Q. Song and P. Tsiakaras, *Appl. Catal. B*, **63**, 187 (2006).
2. X. Y. He, C. G. Hu, Q. N. Yi, X. Wang, H. Hua, and X. Y. Li, *J. Electrochem. Soc.*, **160**, F566 (2013).
3. J. M. Léger, *J. Appl. Electrochem.*, **31**, 767 (2001).
4. K. Y. Chan, J. Ding, J. Ren, S. Cheng, and K. Y. Tsang, *J. Mater. Chem.*, **14**, 505 (2004).
5. T. Kawaguchi,W. Sugimoto, Y. Murakami, and Y. Takasu, *J. Catal.*, **229**, 176 (2005).
6. J. N. Tiwari, R. N. Tiwari, and K. L. Lin, *ACS Appl. Mater. Interfaces*, **2**, 2231 (2010).
7. I. S. Park, B. Choi, D. S. Jung, and Y. E. Sung, *Electrochim. Acta*, **52**, 1683 (2006).
8. X. Wang, C. G. Hu, Y. F. Xiong, H. Liu, G. J. Du, and X. S. He, *J. Power Sources*, **196**, 1904 (2011).
9. I. S. Park, K. W. Park, J. H. Choi, C. R. Park, and Y. E. Sung, *Carbon*, **45**, 28 (2007).
10. A. C. C. Tseung and K. Y. Chen, *Catal. Today*, **38**, 439 (1997).
11. B. L. Garcia, R. Fuentes, and J. W. Weidner, *Electrochem. Solid State Lett.*, **10**, B108 (2007).
12. B. Moreno, E. Chinarro, J. L. G. Fierro, and J. R. Jurado, *J. Power Sources*, **169**, 98 (2007).
13. A. L. Santos, D. Profeti, and P. Olivi, *Electrochim. Acta*, **50**, 2615 (2005).
14. T. Okanishi, T. Matsui, T. Takeguchi, R. Kikuchi, and K. Eguchi, *Appl. Catal. A*, **298**, 181 (2006).
15. L. Jiang, G. Sun, Z. Zhou, S. Sun, Q. Wang, S. Yan, H. Li, J. Guo, B. Zhou, and Q. Xin, *J. Phys. Chem. B*, **109**, 8774 (2005).
16. H. Chhina, S. Campbell, and O. Kesler, *J. Power Sources*, **161**, 893 (2006).
17. M. S. Saha, R. Li, and X. Sun, *Electrochem. Commun.*, **9**, 2229 (2007).
18. H. L. Pang, J. P. Lu, J. H. Chen, C. T. Huang, B. Liu, and X. H. Zhang, *Electrochim. Acta*, **54**, 2610 (2009).

19. H. L. Pang, X. H. Zhang, X. X. Zhong, B. Liu, X. G. Wei, Y. F. Kuang, and J. H. Chen, *J. Colloid Interf. Sci.*, **319**, 193 (2008).
20. A. Kolmakov and M. Moskovits, *Annu. Rev. Mater. Res.*, **34**, 151 (2004).
21. H. L. Zhang, D. Z. Wang, C. G. Hu, X. L. Kang, and H. Liu, *Sensor. Actuat. B-Chem.*, **184**, 288 (2013).
22. T. J. Schmidt, H. A. Gasteiger, G. D. Stab, P. M. Urban, D. M. Kolb, and R. J. Behm, *J. Electrochem. Soc.*, **145**, 2354 (1998).
23. A. Pozio, M. De Francesco, A. Cemmi, F. Cardellini, and L. Giorgi, *J. Power Sources*, **105**, 13 (2002).
24. H. L. Zhang, C. G. Hu, X. S. He, H. Liu, G. J. Du, and Y. Zhang, *J. Power Sources*, **196**, 4499 (2011).
25. F. Y. Xie, Z. Q. Tian, H. Meng, and P. K. Shen, *J. Power Sources*, **141**, 211 (2005).
26. T. Matsui, K. Fujiwara, T. Okanishi, R. Kikuchi, T. Takeguchi, and K. Eguchi, *J. Power Sources*, **155**, 152 (2006).